Enabling Patient- and Teleoperator-led Robotic Physiotherapy via Strain Map Segmentation and Shared-authority

Balvert, S.; Prendergast, J.M.; Belli, I.; Seth, A.; Peternel, L.

DOI
10.1109/Humanoids53995.2022.10000234

Publication date
2022

Document Version
Final published version

Published in
Proceedings of the 2022 IEEE-RAS 21st International Conference on Humanoid Robots (Humanoids)

2022 IEEE-RAS 21st International Conference on Humanoid Robots (Humanoids)
November 28-30, 2022. Ginowan, Japan.

Enabling Patient- and Teleoperator-led Robotic Physiotherapy via Strain Map Segmentation and Shared-authority

Stephan Balvert[1], J. Micah Prendergast[1,*], Italo Belli[1,2], Ajay Seth[2], and Luka Peternel[1]

***Abstract*— In this work, we propose a method for monitoring and managing rotator-cuff (RC) tendon strains in human-robot collaborative physical therapy for shoulder rehabilitation. We integrate a high-resolution biomechanical model with a collaborative industrial robot arm and an impedance controller to provide feedback to a human subject, therapist or both, which prevents the subject from entering unsafe poses during rehabilitation. The biomechanical model estimates RC tendon strain as a function of human shoulder configuration, muscle activation and applied external forces. Subject- and injury-specific data are model estimates of strain that compose *strain maps*, which capture the relationship between the RC strains and movement of the shoulder degrees of freedom (DoF). High-strain regions of the strain map are identified as unsafe zones by clustering and ellipse fitting to smoothly demarcate these zones. These unsafe areas, which reflect increased risks of (re-)injury, are used to define parameters of an impedance controller and reference pose for real-time biomechanical safety control. Using strain maps we demonstrate both safe patient-led movements and teleoperated movements that prevent the subject from entering unsafe zones. In the teleoperated case, the physical therapist leads the patient remotely using a haptic device. The proposed method has the potential to improve the safety, range of motion, and volume of activity that a patient receives through robot-mediated physical therapy. We validated our approach using three experiments that demonstrate shoulder joint torques of less than 1 Nm during free motion with larger torques occurring only when the subject was asked to actively push into the unsafe boundary or, in the case of teleoperation, to resist the physical therapist.**

I. Introduction

Musculoskeletal injuries attributed to accidents, recreation and/or general wear-and-tear due to ageing are the leading cause of living with a disability and being unable to work. Of these injuries, a shoulder rotator-cuff (RC) tear is one of the most common, with an estimated prevalence rate of 22.1% in the general population and over 50% for those older than 60 [1]. To restore shoulder mobility and functionality following RC injuries, a patient must undergo a lengthy and expensive physiotherapy process.

Due to the complexity of the shoulder joint, and a lack of quantitative insights into re-injury risks, existing practices of RC physiotherapy typically involve rather conservative movements even when performed by expert physiotherapists [2]. The conservative nature of such therapy means that the intensity of treatment delivered is limited in terms of the range of motion (RoM). Overly restricting RoM can slow down the healing process while safely increasing RoM improves it along with with the completeness of recovery [3]. Furthermore, RC therapy itself can be quite strenuous for physiotherapists who typically handle many patients each day, and are limited to assisting/treating one patient at a time. A promising alternative to the traditional approach is robotic-assisted rehabilitation.

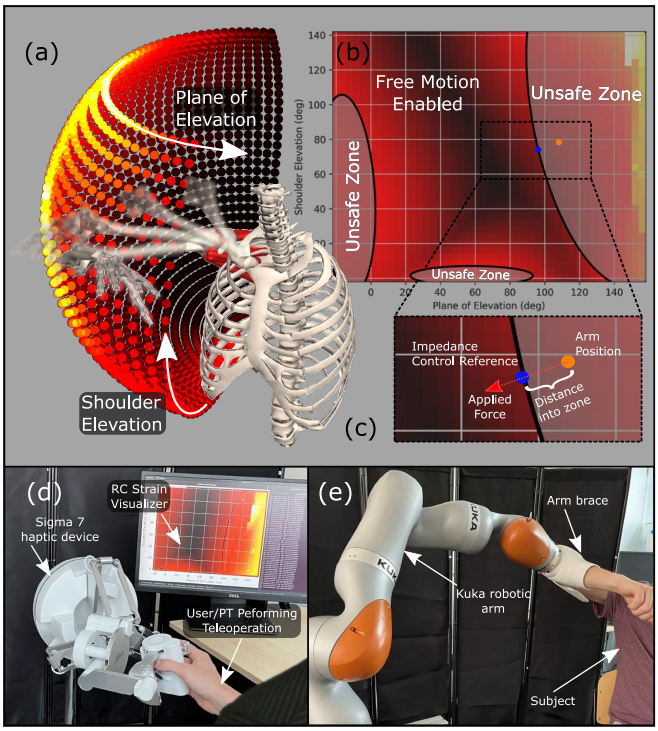

Fig. 1: An overview of the complete high strain avoidance system. (a) OpenSim shoulder model and rotator-cuff (RC) strain map are overlaid. (b) One RC strain map is shown with unsafe (high strain) zones labeled. (c) Impedance control to push subjects out of unsafe zones is shown. (d) The sigma.7 haptic device and the strain map visualizer can be used for safely teleoperating the system. (e) The Kuka LBR iiwa robotic arm is used to control the subject so that they cannot reach poses that would result in unsafe RC tendon strains.

The majority of existing robotic rehabilitation devices are custom-built robots and exoskeletons [4], [5]. The main advantage of such devices is that they can be specialised for treating specific injuries/joints in terms of the mechanical design, required payload, RoM, and degrees of freedom (DoF) [6]–[8]. Nevertheless, custom-built robots and exoskeletons are typically overspecialised and expensive, which makes it difficult for them to be used for multiple purposes and on a larger scale. On the other hand, mass-produced industrial collaborative robots are typically less expensive and are designed to be versatile multi-purpose devices that are certified for safe physical human-robot interaction (pHRI).

Authors are with the Department of Cognitive Robotics[1] and the Department of BioMechanical Engineering[2], Delft University of Technology, Delft, The Netherlands
*Corresponding author (j.m.prendergast@tudelft.nl)

2022 IEEE-RAS 21st International Conference on Humanoid Robots (Humanoids) | 979-8-3503-0979-9/22/$31.00 ©2022 IEEE | DOI: 10.1109/HUMANOIDS53995.2022.10000234

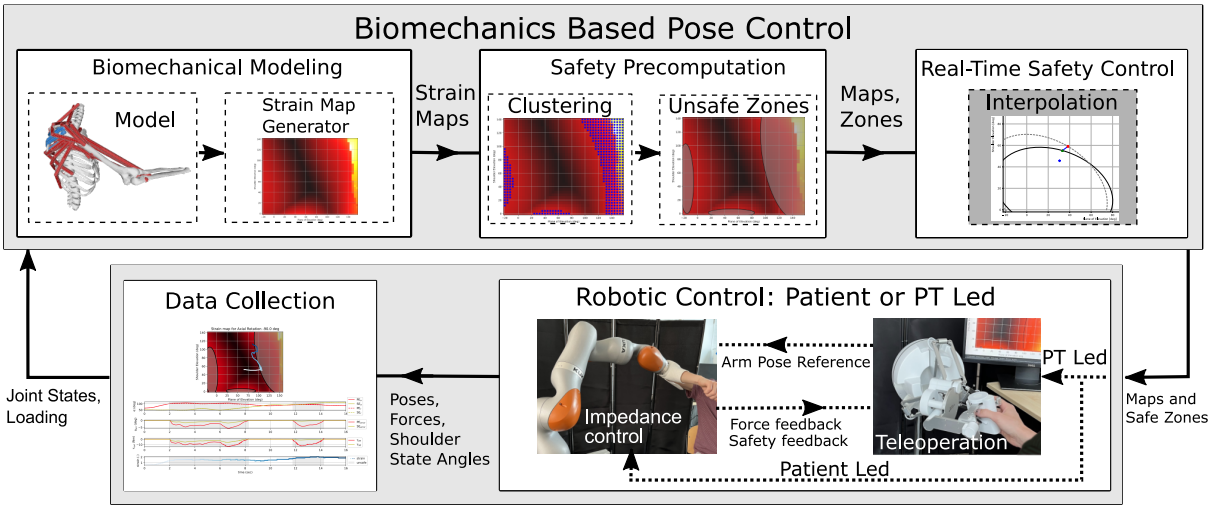

Fig. 2: Workflow of the biomechanics aware robotic system for delivering physical therapy. The biomechanical model is used to generate maps of muscle strains. Clustering-based segmentation is performed to determine unsafe pose regions and ellipse fitting is done to simplify these "unsafe zones". Additional interpolation is done to allow for smooth map transitions during real-time changes to axial-rotation. These maps and corresponding safe zones are then used either directly by the robotic control system during patient-led activities or by the haptic feedback system for guiding and restricting the physiotherapist as they lead the patient. Robot position and force measures are fed back to the biomechanical model to update its current state. Data is collected from the robot for further evaluation.

Previous research on the safety of collaborative robots during pHRI has predominantly focused on external safety in terms of collision detection and avoidance [9], [10], soft robots [11], [12], compliant actuators [13], influence of robot joint configuration on collision injury [14], awareness of potential injury caused by human-robot collisions [15], [16], and conservative force/velocity limits [17]. However, characteristics related to robots' external safety are often insufficiently consistent with medically observed injuries [18], thus some insight into the internal states of the human body is needed for a more complete perception of safety.

To evaluate the characteristics related to the internal safety of collaborating humans during pHRI in real-time, several approaches have used heuristic ergonomics for ergonomic working postures [19], [20], which are based on methods such as Rapid Upper Limb Assessment (RULA) [21] and Rapid Entire Body Assessment (REBA) [22]. The final scores of RULA and REBA can provide a quick assessment of the posture of relevant limbs, providing an indication of the level of musculoskeletal disorders (MSD) risk. Unfortunately, these heuristics are difficult to generalise for specific humans, tasks, and conditions, and do not provide detailed information about the inner workings of the musculoskeletal system. This problem can be solved by using musculoskeletal models, which can account for patient-specific parameters and give an accurate estimate of the actual internal properties of the human body in real-time; such as (static) joint loading [23], muscle fatigue [24], muscle comfort [25], and muscle manipulability [26]. While promising, these methods used collaborative robots for pHRI in workplace tasks rather than physiotherapy.

A few recent studies focused on using off-the-shelf collaborative robotic arms for shoulder rehabilitation. For example, a collaborative robotic arm was used for upper arm rehabilitation, where the robot measured force, position, and electromyography (EMG) data from various sensory systems [27]. In a similar manner, a collaborative robotic arm was used to perform shoulder rehabilitation, where the control was based on the measurement of arm pose and muscle activity through EMG [28]. While these examples were limited to direct pHRI, the method in [29] used teleoperation to enable the human physiotherapist to guide the collaborative robotic arm performing the therapy remotely. The methods in [27], [28] did not incorporate musculoskeletal models and had to rely on external measurements, thus like human physiotherapists, they had limited insight into the inner workings of the musculoskeletal system. The method in [29] did use a musculoskeletal model to guide the therapy to some degree. However, musculoskeletal models are composed of numerous underlying variables that are difficult to interpret, thus an abstraction that is suitable for an intuitive representation for use by human physiotherapists or in effective real-time control is missing.

To address this gap, our previous work [30] demonstrated an abstraction of a complex musculoskeletal model, called the "strain maps", that provide an intuitive representation of the RC tendon strains and are used in effective real-time control. These maps give the robot controller a high-resolution estimate of muscle strains in the joint space. The strain maps were generated for the four RC muscles and the robot trajectory was planned to minimise the risk of re-injury while maximising RoM. Nevertheless, the study was limited to planned robot trajectories more suitable for the initial stage of therapy where solely passive movements are utilized.

In this study, we propose a strain-based control method for physiotherapy using a collaborative robot that goes beyond planned trajectories. The proposed approach (see Fig. 1 for concept overview) enables the active involvement of the

patient, in which they can perform movements themselves to maximise RoM, or be guided by a physiotherapist. In both cases, the controller for the robot (and haptic device in the case of teleoperation) acts as a safeguard to prevent the patient from reaching dangerous poses or "unsafe zones". Expanding on our previous work [30], where the planned trajectories only demonstrated motion in the plane of elevation (PE) and shoulder elevation (SE) degrees of freedom, in this work we also allow for axial rotation (AR) and incorporate all associated control complexity.

We validate the patient-led approach on a Kuka LBR iiwa collaborative robotic arm serving as the robotic physiotherapist, while a human performs movements on their own within the safety bounds defined by a strain threshold. Similarly, we demonstrate the physiotherapist-led approach using a haptic device (sigma.7, Force Dimension, Nyon Switzerland) to remotely operate the robot while the therapist receives visual and haptic feedback based on these unsafe zones and any applied forces or resistance from the patient in a share-authority fashion.

II. Methods

The methods section is divided into four sub-sections. II-A gives an overview of the involved systems and relevant coordinate frames, II-B presents the biomechanical model that is adopted for modeling the patient and the way in which safe human positions are defined, II-C details the control algorithm that we propose to allow the robot to deliver safe physiotherapy to the patients, and II-D explains the implementation of our teleoperation approach to physiotherapy. As a reference, a block diagram overview of the proposed approach is shown in Fig. 2.

A. Coordinate Frames

To enable the robot to physically interact with the patients and prevent them from accidentally re-injuring themselves, a custom arm brace was mounted on the robot end-effector and worn by the patient, see Fig. 1. The brace, shaped like an "L", limited the movement of the patients and allowed the robot to know the position in space of their elbow, since this was translated by a known quantity with respect to the end-effector pose $x_{ee} \in \mathbb{R}^6$, measured by the robot's encoders. We define the following frames (see Fig. 3):

- *shoulder frame*: centered on the humeral head of the patient, its x-axis lies in the frontal plane of the patient body and points towards the left shoulder, while the z-axis is parallel to the sagittal plane and pointing upwards;
- *arm frame*: centered on the elbow joint, the x-axis points towards the wrist and the z-axis towards the shoulder;
- *arm brace frame*: aligned with the arm frame. The arm is mounted so that the z-axis of the robot end-effector and the z-axis of the arm brace frame coincide.

During the experiments, participants (acting as patients) were instructed not to move their torso, so that the shoulder frame was considered to remain fixed over time. In this way, it was possible to establish a constant transformation that linked the state of the glenohumeral joint to the position and orientation of the arm frame. The system was therefore always aware of the biomechanical condition of the subjects, who were either free to explore their shoulder's RoM autonomously or were guided in the rehabilitation exercises by the physiotherapist through teleoperation.

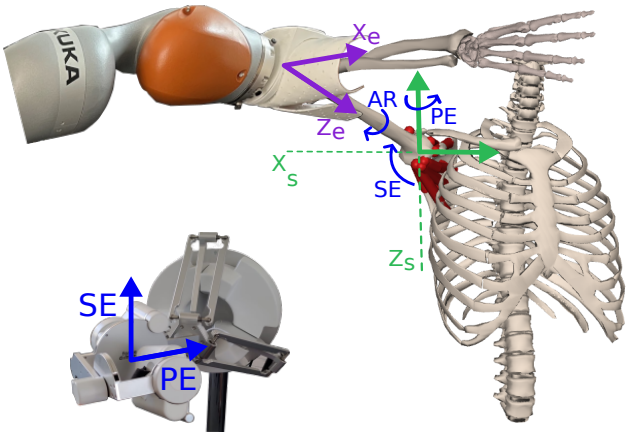

Fig. 3: Overview of the coordinate systems used: shoulder frame (green), with the origin centered on the glenohumeral joint; DoF of the glenohumeral joint (blue) and their mapping to the sigma.7 device; robot's end-effector frame (purple). When the patient is wearing the arm brace, the elbow frame coincides with the end-effector frame.

B. Biomechanical Model and Safety

To suitably represent the patient with a biomechanical model, we leveraged the shoulder model presented in [31], [32]. This model describes the right shoulder joint with a high degree of fidelity, including the four rotator cuff muscles: subscapularis, teres minor, supraspinatus and infraspinatus. By means of the open-source musculoskeletal modelling tool OpenSim [33], [34] the full RoM of the human shoulder can be simulated and the strains of the RC muscles for various robot-mediated human poses computed. In particular, we focus on the value of the induced tendon strain level ϵ, which is indicative of the risk of tearing or re-injury for the muscle, and is defined as a dimensionless number as follows

$$\epsilon = \frac{l^T - l^0}{l^0} \cdot 100\% \tag{1}$$

where l^T and l^0 are the tendon length and slack length (i.e., the length at which the tendon starts to stretch) respectively. As previously mentioned, we restrict our analysis to the influence that the 3 DoF of the human glenohumeral joint have on the resulting strain level, thus effectively defining the shoulder state vector as

$$\alpha = [\text{AR} \quad \text{PE} \quad \text{SE}] \tag{2}$$

where the values are limited to be $-90° \leq AR \leq 90°$, $-20° \leq PE \leq 160°$ and $0° \leq SE \leq 144°$ to include only feasible poses. The humerus of the model was posed in all combinations of the 3 shoulder state variables, using $4°$ increments, and the corresponding strain values are computed offline. For a given value of α, we grouped the strain

levels into a single metric consisting of the maximum strain experienced among the RC muscles, which allows us to avoid large strains in all four tendons. To accommodate specific injuries of actual patients in the future, this value can be adjusted and/or applied to only the map of the tendon that has been injured (i.e., the infraspinatus map). By selecting an appropriate value of strain as a threshold, we classified each pose of the human arm as "safe" or "unsafe", thus minimizing the risk for re-injury during the rehabilitation exercises. The strain threshold was set conservatively to be 2.4% under the assumption that larger strains even within the elastic deformation range of the tendons (4-8%) might still exceed the safe limits for a tendon that has been surgically repaired [35]. This threshold was applied on the combined strain map that includes only the maximum strain from the four RC tendons.

For this biomechanical information to be integrated into the robot control, we broke down the 3-dimensional space in which α is defined into 2-dimensional "layers" (where AR is fixed): these are referred to as *strain maps* in the current work. When AR changes, a new map is considered. For each one of these maps, we defined unsafe clusters (or *zones*) where the strain level is above the safety threshold, see Fig. 4. First, an equivalent map was retrieved by retaining just the points $\{$PE,SE$\}$ whose strain is greater than the threshold. As a second step, the unsafe points are clustered using the Density-Based Spatial Clustering of Applications with Noise (DBSCAN) algorithm [36], which was chosen because of its ability to cope with an unknown number of clusters, its ability to identify non-spherical shapes and its low computational cost. These characteristics are desirable since they ease the pre-computation of the clusters among the strain maps without the need for supervision. When the unsafe zones have been identified, they are approximated as minimum-volume enclosing ellipses (MVEEs). This representation of the unsafe zones was chosen as it allows for more efficient computation of the control references (see II-C), at the acceptable cost of constraining the allowed RoM to be possibly more conservative, but still safe.

C. Strain-Map-Based Impedance Control

To integrate the strain-map-based safety into the robot control in real-time, at every timestep t we need to:

1) find the current shoulder state vector α_t;
2) leverage the strain maps to perform a biomechanical safety check;
3) send commands to the robot.

A Cartesian impedance controller is used to control the interaction force exerted by the robot on the patient:

$$\boldsymbol{F}_{imp} = \boldsymbol{K}(\overline{\boldsymbol{x}}_{ee} - \boldsymbol{x}_{ee}) + \boldsymbol{D}(\dot{\overline{\boldsymbol{x}}}_{ee} - \dot{\boldsymbol{x}}_{ee}), \qquad (3)$$

where $\boldsymbol{F}_{imp} \in \mathbb{R}^6$ is the interaction force/torque vector acting from the robot to the patient, $\boldsymbol{K}, \boldsymbol{D} \in \mathbb{R}^{6\times6}$ are the desired stiffness and damping matrices in Cartesian space, and $\overline{\boldsymbol{x}}_{ee}$ and $\boldsymbol{x}_{ee} \in \mathbb{R}^6$ are the reference pose and the measured actual pose of the end-effector, respectively. $\boldsymbol{K}$ is defined to prescribe the desired Cartesian and rotational

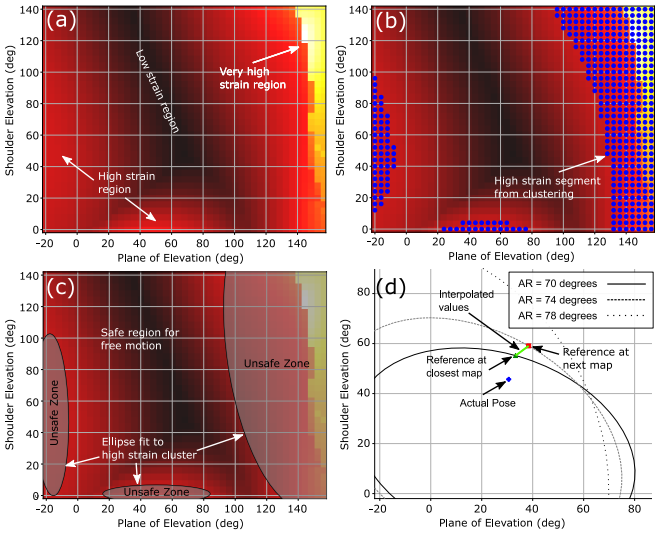

Fig. 4: Identification and segmentation of unsafe zones. (a) A raw strain map at each axial rotation pose is first generated, (b) DBSCAN is used to cluster high strain points together within the map, (c) ellipses are fit to these segments to serve as simplified boundaries which must be used in real-time by the robot to ensure safe motion of the patient. (d) multiple axial rotation maps are combined by interpolating between adjacent ellipses so as to ensure smooth force changes during axial rotation.

stiffness and its value was determined iteratively, to ensure subjects would be deterred from crossing unsafe zone boundaries. Based on this stiffness, $\boldsymbol{D}$ was obtained using the double diagnolisation design technique [37].

The references for (3) are adjusted according to a safety check based on α_t, where we assess whether the shoulder state lies in an unsafe zone in the current strain map (AR is virtually fixed, and strain values depending on the current PE and SE are considered). If this was the case, the closest safe point lying on the elliptic contour of the zone was estimated in real-time with Brent's approach [38] and set as a reference point. To ensure that the patient was repositioned to the new reference pose, the impedance control stiffness matrix was set to high stiffness ($\boldsymbol{K}_{hi}$), and the damping matrix was adjusted accordingly. This results in a control force $\boldsymbol{F}_{imp}$ that pushes the patient perpendicularly towards the zone boundary, ensuring minimal penetration into the zone itself. In all other cases where α_t does not correspond to an unsafe strain, the reference point was set to the current coordinates $\{$PE$_t$, SE$_t\}$ so that no resistive force is generated by the impedance controller.

Similarly, a second safety check addressed the problem that, even if α_t was safe in the current strain map, slight changes in the AR value could make it unsafe in an adjacent one (by changing the value of AR unsafe zones change as well). This check only affects the AR angle, and spans the third dimension of the shoulder state vector space. In the case in which AR was approaching a value that would entail excessive strains, the impedance control parameters $\boldsymbol{K}$ and $\boldsymbol{D}$ were set to high values as in the previous/unsafe case. This results in a torque on the z-axis of the robot end-effector that guides the subject towards the safe strain map, hence acting only along the AR coordinate.

With the control methodology formulated above, the pa-

tients could freely explore the RoM of their glenohumeral joint, while the robot implemented limitations on their motion based on quantitative knowledge of their internal safety, expressed in terms of RC muscle strains. It must be noted that, as described in II-B, AR is a quantity that varies continuously, while the strain maps were precomputed with a fixed discretization. This means that the patient will never be exactly on one strain map, but between two adjacent ones. Therefore, smooth transitions between maps was guaranteed by calculating the closest safe points for both maps and retrieving the correct reference point by linear interpolation as a function of AR (see Fig. 4 (d)). Finally, we also leveraged gravity compensation such that the jointed weight of the brace+robot system was not sustained by the subjects themselves.

D. Tele-Physiotherapy through Haptic Device

To demonstrate the utility of our method, we implemented a second modality in which a patient received therapy from a physiotherapist (PT) by leveraging the metric of biomechanical safety introduced in II-B in terms of strains. In this case, we allowed for a shared-authority control of the patient's movement, which was facilitated by the use of a haptic device with which the PT could interact with the patient. The use of the haptic teleoperation interface makes it possible for a PT to move the patient's elbow through the sigma.7 gripper, as the movement of the haptic device is transferred to the Kuka end-effector directly. By limiting the haptic device's RoM on the basis of the value of α, the PT experiences a repulsive force field in case an unsafe zone is being entered. The feedback force that the PT experiences can be formalized as follows:

$$\boldsymbol{F}_{fb} = \boldsymbol{F}_{zone} + k_p(\overline{\boldsymbol{x}}_{PT} - \boldsymbol{x}_{ee}) + k_v\dot{\overline{\boldsymbol{x}}}_{PT} \qquad (4)$$

where the first term implements biomechanical safety as explained above. The second term introduces a force proportional to the error between the commanded pose $\overline{\boldsymbol{x}}_{PT}$ for the robot and the actual end-effector pose, so that potential movements or resistances on the patient side are reflected in a feedback force for the PT. The last term in (4) represents a viscosity force depending on the velocity of the commanded movement that is generated, to prevent the PT from unwillingly generating excessively fast movements during therapy.

During the experiments, the experimenter monitored the subject's position within the strain map in real-time using a GUI visualization on a monitor. This visualization also showed the unsafe zones overlayed onto the map to enable easy navigation for the experimenter.

III. Results

In this section we present results for the two modalities within the proposed method. One healthy individual acts as subject/patient for the following experiments. By considering a scaled version of the OpenSim model, strain maps were generated and divided into safe and unsafe zones by selecting the strain threshold to be 2.4%. In III-A a first simpler case

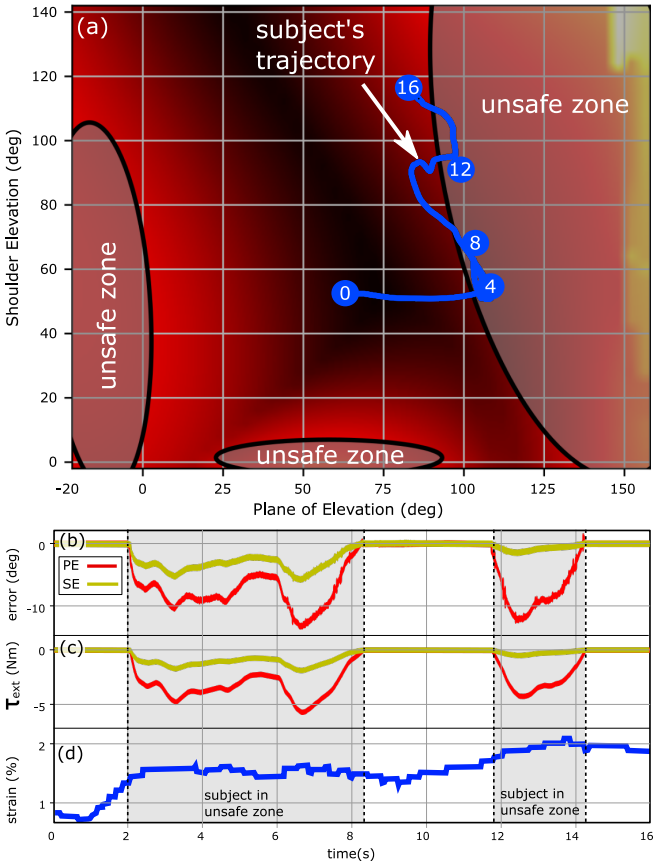

Fig. 5: An example experiment where Axial Rotation has been fixed. (a) The trajectory is shown with time stamps in seconds indicated by the enumerated blue circles. (b) pose error used by the impedance controller is shown for those times when the subject has entered the unsafe zone. (c) Joint torques on the subject's shoulder as calculated from the end-effector force of the robot are shown. (d) estimated tendon strain based on the strain map.

is demonstrated, where the subject interacted autonomously with the robot, but the axial rotation of the arm is locked. This case is extended in III-B by leaving the subject-robot interaction unconstrained. In both cases the subject was sitting on a normal chair, and the robot was moved to its initial position so the custom arm brace described above could be worn comfortably. The movements that were performed were projected on the strain map that best represented the current state of the subject's shoulder, and a screen was used to provide visual information allowing safe exploration of the shoulder range of motion. The visual display was updated at 30 Hz, while the robotic control loop ran at 200 Hz. We then integrated the sigma.7 into the experimental setup to test our teleoperation system. These results are given in III-C. Overall, this study was approved by the Human Research Ethics Committee of Delft University of Technology.

A. AR locked

First, we considered the case in which the subject movement was constrained to lie on one strain map only. By locking the rotation of the end-effector about its z-axis, the resulting trajectory is visualized on a single strain map, since only PE and SE can change. In such a way, interpretation and discussion of the results become possible in a single 2D

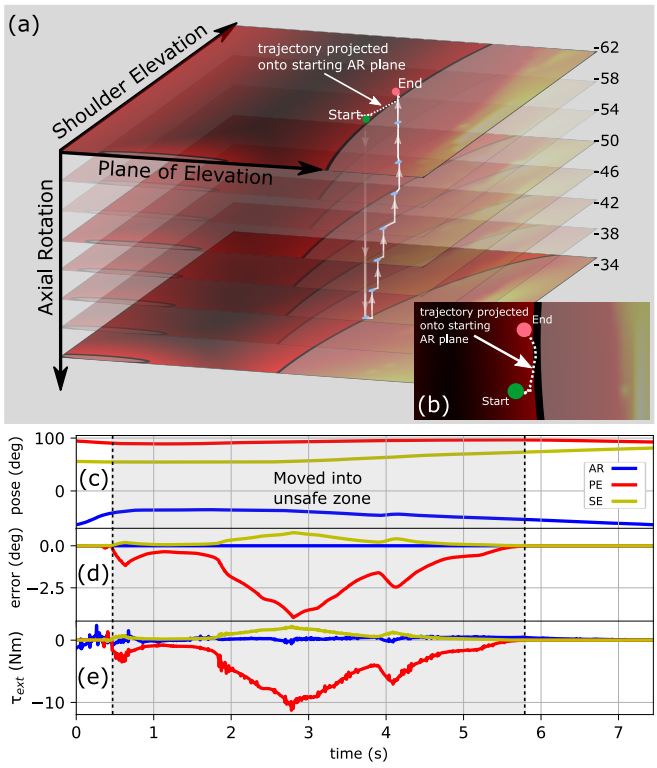

Fig. 6: An example of a full three degree of freedom motion experiment is shown. (a) the corresponding strain maps representing the change of axial rotation are shown here as partially transparent so that the trajectory can be seen. (b) the full trajectory is plotted just on the original axial rotation map for ease of visualization. (c) the full shoulder pose of the subject is shown (d) the error used by the impedance controller is shown for the time in which the subject is in an unsafe zone (e) joint torques as calculated from the end-effector force.

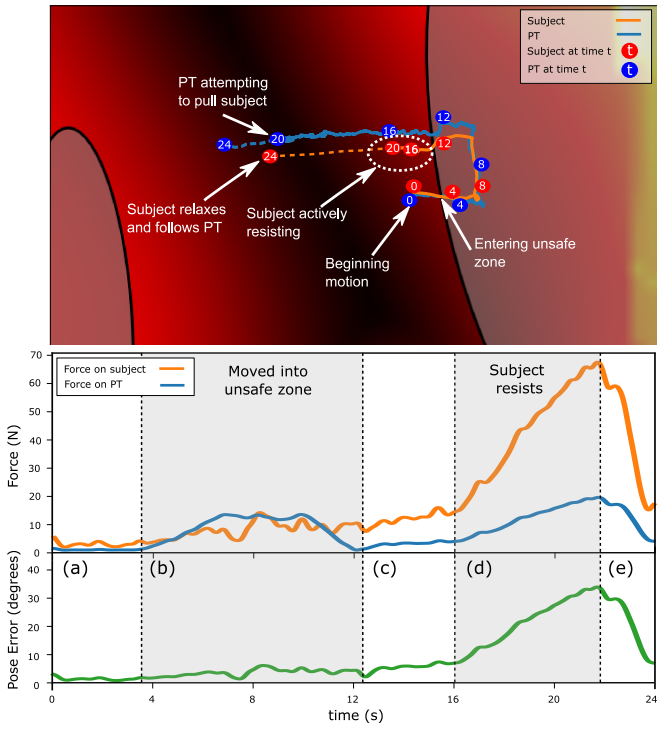

Fig. 7: An example teleoperation experiment is shown along with the force and pose data. The top image shows the strain map and trajectory traveled with the time indicated by the numbers along the subject and PT's trajectories. (a) Initially the subject follows the PT and overall forces are low. (b) as the PT pushes into the unsafe zone they feel the force feedback from the zone boundary. (c) Both the subject and PT have exited the unsafe zone. (d) The subject has been asked to actively resist at this point while the PT attempts to pull them along. (e) The subject relaxes and once again begins to follow the PT.

plot. The references for the impedance controller formulation as in (3) are computed in real-time, depending on the interaction with unsafe zones. In Fig. 5 a selected trajectory of 16 seconds was visualized, during which the subject interacted with one unsafe zone during their exploration of the rehabilitation space: when the current shoulder state α_t became unsafe, the controller reference was shifted to the closest point on the border of the ellipse, producing robot torques that encouraged the subject to navigate, once again, to a safe region. The positional and rotational stiffness for the controller was tuned to be $k_{hi\_p} = 800$ N/m and $k_{hi\_r} = 30$ Nm/rad when inside an unsafe zone, and $k_{lo\_p} = {}^{k_{hi\_p}}/_2$ and $k_{lo\_r} = {}^{k_{hi\_r}}/_2$ otherwise. Note that as shown in Fig. 5 (d), the percentage of strain within the zone may be lower at some points than the strain outside of the zone. This is because the unsafe zone represents a somewhat conservative estimate and as such breaching the zone itself does not necessarily put the patient at risk. At no point during these experiments did the subject ever exceed the strain threshold of 2.4%.

B. Free interaction results

This experiment showcases our proposed use of a patient-led robotic-assisted rehabilitation. No constraints were prescribed on the motion of the shoulder by the subject, so that α could freely vary inside their feasible biomechanical range of motion. In the reported results, the movement happened through 8 different strain maps: the trajectory travelled on each map and the strain map themselves are shown in Fig. 6. Initially, the subject axially rotated 28 degrees, intentionally forcing themselves into an unsafe zone. The subject then rotated back slowly while also moving along the other two DoF, until they eventually returned to the original axial rotation position.

C. Teleoperation results

The test reported here for the use of strain-map-based safety demonstrates the effectiveness of the teleoperation approach. One of the authors acted as the PT operator, and drove the movements of the subject's elbow. To demonstrate different scenarios, the movement began in the safe-strain region, and then the subject was driven towards an unsafe zone (Fig. 7). As the initial motion is slow and safe, the operator did not feel significant feedback force, as expected from (4). When the unsafe zone was hit, the operator experienced a repulsive force pointing towards the safe region. For illustration purposes, the operator navigated briefly inside the unsafe region, and then drove the subject away from it. Note that, because it requires some force for the PT to push into this zone, there was some oscillation by the PT that also resulted in some increased forces for the subject. At this point, the subject was instructed to resist the end-effector force, such that the reference trajectory and the

actual trajectory diverged, and this generated a feedback force for the operator.

IV. Discussion

The results shown represent a step forward in the biomechanical-aware safe interaction between robots and humans. They support our claim that it is possible to deliver sophisticated physiotherapy by employing commercially available collaborative robots that, while not designed primarily for this aim, can be used as a part of reliable physiotherapy tools or systems when integrated with biomechanics-based feedback and safe control modalities. Moreover, such off-the-shelf collaborative robotic systems natively grant various safety features for pHRI as they already respect rigorous standards. This is a significant benefit in comparison with custom-built rehabilitation robotic platforms or exoskeletons, where similar features must still be implemented and standardized for each new individual device. We demonstrated that the strain maps that we generated are suited for a patient-led therapy that could be useful to assist during later stage shoulder rehabilitation, extending the purely robotic-driven approach that we presented in [30], which was suited only at the very early stages of therapy.

The very same strain maps also enable the delivery of expert treatment in the case in which a professional physiotherapist (rather than the patient on their own) interacts with the robot. The approach we presented enables the PT to visualize in real-time the quantitative strain that the therapy is generating in the patient's tendons, possibly leading to a more efficient and safer therapy overall. The way in which the PT interacts with the patient during teleoperation relieves them from physical fatigue, since it is primarily the robot that supports the weight of the patient's arm. Future efforts will also enable full arm-weight compensation during the patient-led exercises.

Both the modalities that we demonstrated can be considered safe for the patient interacting with the robot as the forces/torques generated by the robot are extremely low (less than 1 Nm) when movement happens within the safe zone (see Figs. 5,6,7). The same results show that the forces/torques exerted on the patient increase when an unsafe zone is entered: the value reached is proportional to the amount of penetration into the unsafe zones, and the increase in this value is guaranteed to be smooth due to the interpolation performed on the reference point for the Cartesian controller, as described in Section II-C. Higher forces are observed in the case in which the subject actively resisted the PT, as reported in Section III-C: this is not considered an issue as it is assumed that the operator/PT can supervise the patient, hence modifying the commanded trajectory when they assess that the patient is non-compliant. In general, it is expected that intentional patient resistance during robotic therapy is somewhat unlikely or at least no more likely than during conventional therapy. Regardless, the development of a safe strategy to minimize the risk of (re-)injury in cases of active resistance could be beneficial, as it should also be considered that the strain maps will change when the patient's muscle activation increases significantly.

Finally, it is important to include in the biomechanical modeling information regarding the injuries that the patient has suffered or the surgery they have undergone, to generate real patient-specific rehabilitation policies. Currently our maps can be weighted based on which RC-tendon has been injured (and thus which tendon may be most sensitive to large strains), however for the work presented here we assume all RC-tendons are equally at risk.

Our future work will consider how to expand the presented method, for example by allowing the robot to gradually resist the human motion with the goal of allowing the patient to gain the muscular strength they need to effectively complete their rehabilitation by regaining the lost functionalities as much as possible.

V. Conclusion

We present a robotic physiotherapy system that allows a collaborative robot to deliver safe exercises to a patient suffering from a rotator-cuff injury. The presence of the robot enables patient-led rehabilitation movements, and also enables expert rehabilitation guided by a professional PT. Both modalities employ a state-of-the-art biomechanical model to provide RC tendon strain feedback during therapy via the use of strain maps and safe/unsafe zone segmentation. Overall, this system allows the robot and underlying controller to use patient- and injury-specific insights to provide safe control during patient-led or PT-led therapy enabling large RoM activities without risking patient re-injury.

Acknowledgment

The authors would like to thank Irene Beck for her assistance during the testing and experiments conducted for this work.

References

[1] H. Minagawa, N. Yamamoto, H. Abe, M. Fukuda, N. Seki, K. Kikuchi, H. Kijima, and E. Itoi, "Prevalence of symptomatic and asymptomatic rotator cuff tears in the general population: from mass-screening in one village," *Journal of orthopaedics*, vol. 10, no. 1, pp. 8–12, 2013.

[2] T. Proietti, V. Crocher, A. Roby-Brami, and N. Jarrasse, "Upper-limb robotic exoskeletons for neurorehabilitation: a review on control strategies," *IEEE reviews in biomedical engineering*, vol. 9, pp. 4–14, 2016.

[3] H. Østerås and T. A. Torstensen, "The dose-response effect of medical exercise therapy on impairment in patients with unilateral longstanding subacromial pain," *The Open Orthopaedics Journal*, vol. 4, p. 1, 2010.

[4] L. Marchal-Crespo and D. J. Reinkensmeyer, "Review of control strategies for robotic movement training after neurologic injury," *Journal of neuroengineering and rehabilitation*, vol. 6, no. 1, p. 20, 2009.

[5] A. S. Niyetkaliyev, S. Hussain, M. H. Ghayesh, and G. Alici, "Review on design and control aspects of robotic shoulder rehabilitation orthoses," *IEEE Transactions on Human-Machine Systems*, vol. 47, no. 6, pp. 1134–1145, 2017.

[6] A. Schiele and F. C. T. van der Helm, "Kinematic Design to Improve Ergonomics in Human Machine Interaction," *IEEE Transactions on Neural Systems and Rehabilitation Engineering*, vol. 14, no. 4, pp. 456–469, Dec. 2006.

[7] N. Jarrasse and G. Morel, "Connecting a Human Limb to an Exoskeleton," *IEEE Transactions on Robotics*, vol. 28, no. 3, pp. 697–709, Jun. 2012.

[8] B. Kim and A. D. Deshpande, "An upper-body rehabilitation exoskeleton Harmony with an anatomical shoulder mechanism: Design, modeling, control, and performance evaluation," *The International Journal of Robotics Research*, vol. 36, no. 4, pp. 414–435, Apr. 2017.

[9] S. Haddadin, A. De Luca, and A. Albu-Schäffer, "Robot collisions: A survey on detection, isolation, and identification," *IEEE Transactions on Robotics*, vol. 33, no. 6, pp. 1292–1312, 2017.

[10] A. M. Zanchettin, P. Rocco, S. Chiappa, and R. Rossi, "Towards an optimal avoidance strategy for collaborative robots," *Robotics and Computer-Integrated Manufacturing*, vol. 59, pp. 47–55, 2019.

[11] H. Abidi and M. Cianchetti, "On Intrinsic Safety of Soft Robots," *Frontiers in Robotics and AI*, vol. 4, no. FEB, pp. 1–6, 2 2017.

[12] C. Y. Chu and R. M. Patterson, "Soft robotic devices for hand rehabilitation and assistance: A narrative review," *Journal of Neuro-Engineering and Rehabilitation*, vol. 15, no. 1, 2 2018.

[13] Y. Pan, H. Wang, X. Li, and H. Yu, "Adaptive Command-Filtered Backstepping Control of Robot Arms with Compliant Actuators," *IEEE Transactions on Control Systems Technology*, vol. 26, no. 3, pp. 1149–1156, 2018.

[14] S. Hong, C. Cho, H. Lee, S. Kang, and W. Lee, "Joint configuration for physically safe human–robot interaction of serial-chain manipulators," *Mechanism and Machine Theory*, vol. 107, pp. 246–260, 1 2017.

[15] N. Mansfeld, M. Hamad, M. Becker, A. G. Marin, and S. Haddadin, "Safety map: A unified representation for biomechanics impact data and robot instantaneous dynamic properties," *IEEE Robotics and Automation Letters*, vol. 3, no. 3, pp. 1880–1887, 2018.

[16] H. Shin, S. Kim, K. Seo, and S. Rhim, "A Real-Time Human-Robot Collision Safety Evaluation Method for Collaborative Robot," *Proceedings - 3rd IEEE International Conference on Robotic Computing, IRC 2019*, pp. 509–513, 2019.

[17] L. Roveda, S. Haghshenas, M. Caimmi, N. Pedrocchi, and L. M. Tosatti, "Assisting operators in heavy industrial tasks: On the design of an optimized cooperative impedance fuzzy-controller with embedded safety rules," *Frontiers in Robotics and AI*, vol. 6, p. 75, 8 2019.

[18] S. Haddadin, S. Haddadin, A. Khoury, T. Rokahr, S. Parusel, R. Burgkart, A. Bicchi, and A. Albu-Schäffer, "On making robots understand safety: Embedding injury knowledge into control," *International Journal of Robotics Research*, vol. 31, no. 13, pp. 1578–1602, 11 2012.

[19] B. Busch, G. Maeda, Y. Mollard, M. Demangeat, and M. Lopes, "Postural optimization for an ergonomic human-robot interaction," in *IEEE International Conference on Intelligent Robots and Systems*. Vancouver: Institute of Electrical and Electronics Engineers Inc., 9 2017, pp. 2778–2785.

[20] A. G. Marin, M. S. Shourijeh, P. E. Galibarov, M. Damsgaard, L. Fritzsch, and F. Stulp, "Optimizing Contextual Ergonomics Models in Human-Robot Interaction," *IEEE International Conference on Intelligent Robots and Systems*, vol. 1, pp. 8603–8608, 2018.

[21] L. McAtamney and E. N. Corlett, "RULA: A survey method for the investigation of work-related upper limb disorders," *Applied Ergonomics*, vol. 24, no. 2, pp. 91–99, 1993.

[22] L. McAtamney and S. Hignett, "Rapid Entire Body Assessment (REBA)," *Applied Ergonomics*, vol. 31, pp. 201–205, 2000.

[23] W. Kim, J. Lee, L. Peternel, N. Tsagarakis, and A. Ajoudani, "Anticipatory Robot Assistance for the Prevention of Human Static Joint Overloading in Human-Robot Collaboration," *IEEE Robotics and Automation Letters*, vol. 3, no. 1, pp. 68–75, 2018.

[24] L. Peternel, C. Fang, N. Tsagarakis, and A. Ajoudani, "A selective muscle fatigue management approach to ergonomic human-robot co-manipulation," *Robotics and Computer-Integrated Manufacturing*, vol. 58, no. June 2018, pp. 69–79, 2019.

[25] L. F. C. Figueredo, R. C. Aguiar, L. Chen, S. Chakrabarty, M. R. Dogar, and A. G. Cohn, "Human Comfortability: Integrating Ergonomics and Muscular-Informed Metrics for Manipulability Analysis during Human-Robot Collaboration," *IEEE Robotics and Automation Letters*, vol. 6, no. 2, pp. 351–358, 2020.

[26] T. Petrič, L. Peternel, J. Morimoto, and J. Babič, "Assistive arm-exoskeleton control based on human muscular manipulability," *Frontiers in Neurorobotics*, vol. 13, no. May, 2019.

[27] D. Simonetti, L. Zollo, E. Papaleo, G. Carpino, and E. Guglielmelli, "Multimodal adaptive interfaces for 3d robot-mediated upper limb neuro-rehabilitation: An overview of bio-cooperative systems," *Robotics and Autonomous Systems*, vol. 85, pp. 62–72, 2016.

[28] F. Scotto di Luzio, D. Simonetti, F. Cordella, S. Miccinilli, S. Sterzi, F. Draicchio, and L. Zollo, "Bio-cooperative approach for the human-in-the-loop control of an end-effector rehabilitation robot," *Frontiers in neurorobotics*, vol. 12, p. 67, 2018.

[29] M. Tröbinger, A. Costinescu, H. Xing, J. Elsner, T. Hu, A. Naceri, L. Figueredo, E. Jensen, D. Burschka, and S. Haddadin, "A dual doctor-patient twin paradigm for transparent remote examination, diagnosis, and rehabilitation," in *2021 IEEE/RSJ International Conference on Intelligent Robots and Systems (IROS)*. IEEE, 2021, pp. 2933–2940.

[30] J. M. Prendergast, S. Balvert, T. Driessen, A. Seth, and L. Peternel, "Biomechanics Aware Collaborative Robot System for Delivery of Safe Physical Therapy in Shoulder Rehabilitation," *IEEE Robotics and Automation Letters*, vol. 6, 2021.

[31] A. Seth, R. Matias, A. P. Veloso, and S. L. Delp, "A biomechanical model of the scapulothoracic joint to accurately capture scapular kinematics during shoulder movements," *PloS one*, vol. 11, no. 1, p. e0141028, 2016.

[32] A. Seth, M. Dong, R. Matias, and S. Delp, "Muscle contributions to upper-extremity movement and work from a musculoskeletal model of the human shoulder," *Frontiers in Neurorobotics*, vol. 13, 2019. [Online]. Available: https://www.frontiersin.org/articles/10.3389/fnbot.2019.00090

[33] S. L. Delp, F. C. Anderson, A. S. Arnold, P. Loan, A. Habib, C. T. John, E. Guendelman, and D. G. Thelen, "Opensim: open-source software to create and analyze dynamic simulations of movement," *IEEE transactions on biomedical engineering*, vol. 54, no. 11, pp. 1940–1950, 2007.

[34] A. Seth, J. L. Hicks, T. K. Uchida, A. Habib, C. L. Dembia, J. J. Dunne, C. F. Ong, M. S. DeMers, A. Rajagopal, M. Millard, S. R. Hamner, E. M. Arnold, J. R. Yong, S. K. Lakshmikanth, M. A. Sherman, J. P. Ku, and S. L. Delp, "Opensim: Simulating musculoskeletal dynamics and neuromuscular control to study human and animal movement," *PLOS Computational Biology*, vol. 14, no. 7, pp. 1–20, 07 2018. [Online]. Available: https://doi.org/10.1371/journal.pcbi.1006223

[35] K. Robi, N. Jakob, K. Matevz, and V. Matjaz, "The physiology of sports injuries and repair processes," *Current issues in sports and exercise medicine*, pp. 43–86, 2013.

[36] M. Ester, H.-P. Kriegel, J. Sander, X. Xu *et al.*, "A density-based algorithm for discovering clusters in large spatial databases with noise." in *kdd*, vol. 96, no. 34, 1996, pp. 226–231.

[37] A. Albu-Schaffer, C. Ott, U. Frese, and G. Hirzinger, "Cartesian impedance control of redundant robots: Recent results with the DLR-light-weight-arms," in *2003 IEEE International Conference on Robotics and Automation*, vol. 3, 2003, pp. 3704–3709.

[38] R. P. Brent, "Algorithms for minimization without derivatives, chap. 4," 1973.